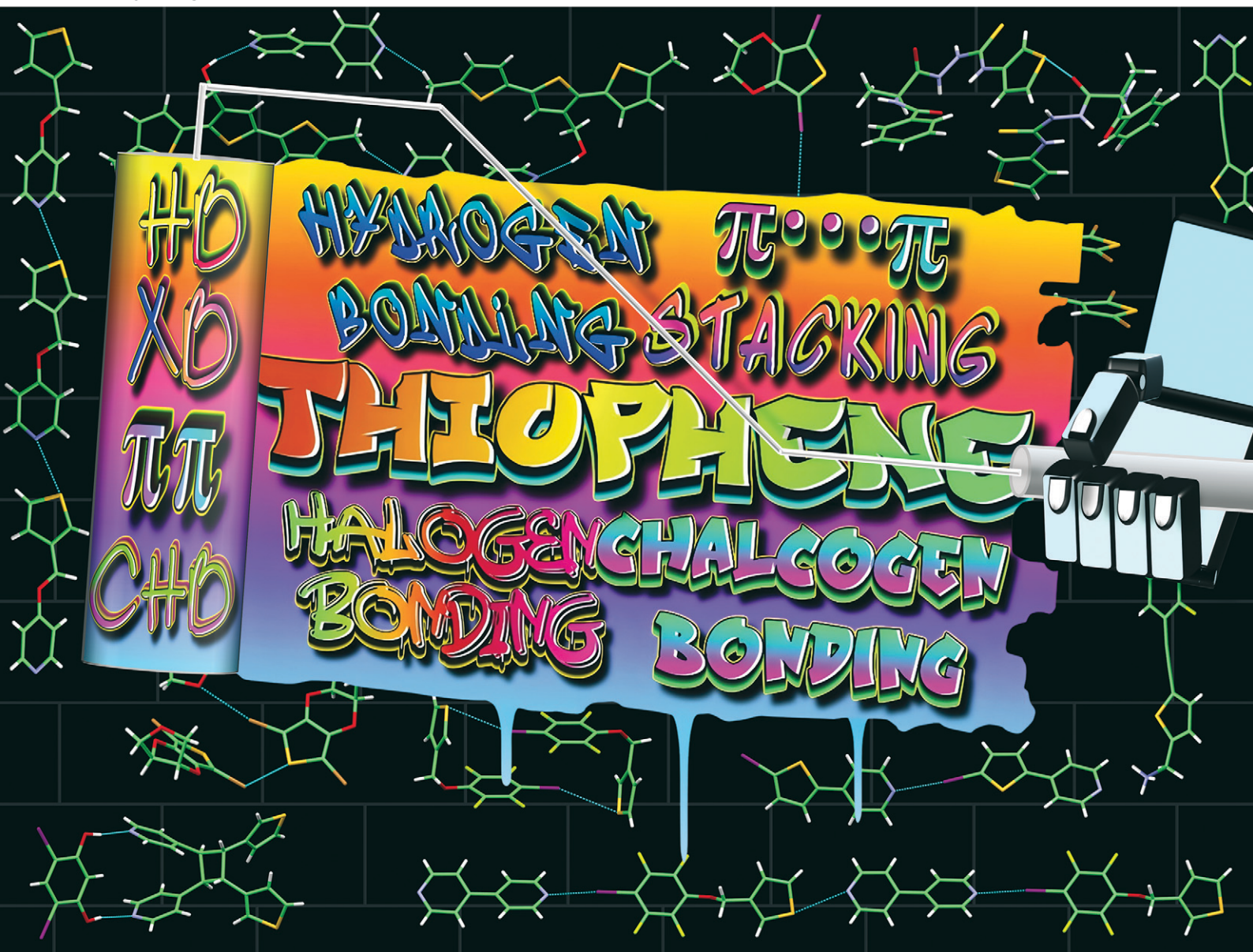


CrystEngComm

rsc.li/crystengcomm



ISSN 1466-8033

HIGHLIGHT

Franck Meyer *et al.*

Harnessing non-covalent interactions in modified thiophenes: structural design and applications in materials and biological sciences



Cite this: *CrystEngComm*, 2025, 27, 736

Harnessing non-covalent interactions in modified thiophenes: structural design and applications in materials and biological sciences

Arvin Sain Tanwar and Franck Meyer  *

Thiophene, a ubiquitous and versatile heterocyclic compound, serves as a cornerstone for modern material sciences due to its distinctive electronic properties and ability to engage in non-covalent interactions, such as $\pi\cdots\pi$ stacking and chalcogen bonding. These interactions can be further enhanced by introducing hydrogen and halogen bond donor groups, rendering functionalized thiophenes highly adaptable and invaluable across a broad spectrum of scientific disciplines. This highlight examines the pivotal role of thiophene-based compounds in advancing organic electronic materials (semiconductors, nonlinear optics, solar cells), sensors, medicinal chemistry (drug design), solid-state reactions (polymerization, mechanochemistry), crystal engineering and the formation of supramolecular helices. The properties and applications of these compounds are predominantly explored through crystallographic data, complemented by microscopy and density functional theory (DFT) studies. From designing advanced functional materials to pioneering new approaches in health and technology, thiophene derivatives exemplify the power of non-covalent interactions in driving innovation.

Received 2nd December 2024,
Accepted 14th January 2025

DOI: 10.1039/d4ce01213e

rsc.li/crystengcomm

Introduction

Thiophene is a five-membered, sulfur-containing heterocyclic compound with a unique aromatic character that makes it exhibit remarkable versatility across various fields.¹ Its distinctive structure and properties have established thiophene as an indispensable building block in organic chemistry, functional materials, and biologically active compounds.^{2,3} In materials science, thiophene-based derivatives play a pivotal role in advancing organic electronics, appearing in forms such as oligomers, polymers, and fused systems.⁴ Each form contributes distinct properties and applications—for instance, thiophene-based polymers enable conductive materials for flexible electronics, while fused thiophene systems enhance the efficiency and stability of organic solar cells. This structural diversity underscores thiophene's potential as a versatile class of materials for technological innovation.^{5,6} Beyond synthetic derivatives, naturally occurring thiophenes represent a rare class of secondary metabolites found in the plants family Asteraceae, *Streptomyces* bacteria, and some species of *Penicillium* and *Aspergillus* fungi.^{7,8} In agriculture, thiophene-based compounds exhibit significant pesticidal activity, including herbicidal effects, protecting crops from pests and

diseases.^{9,10} These structures are also valuable in medicinal chemistry, where they are frequently incorporated into bioactive molecules.¹¹ Thiophene derivatives exhibit a range of notable bioactivities, including antioxidant, antimicrobial, anti-inflammatory, and cytotoxic properties, among others.^{12,13} Additionally, thiophene-based fluorophores are used in cell staining and serve as optical probes for detecting amyloid fibers and membranes, as well as in photodynamic therapy.^{14,15} The study of thiophene chemistry is an active area of research, with ongoing discoveries of new applications and derivatives, underscoring its role in advancing technology and improving health.

Structurally, the thiophene ring, with its sulfur atom exhibiting a dual electronic nature, engages in diverse supramolecular interactions. The sulfur atom's lone pairs make it an electron donor, while its half-filled p-orbitals create σ -holes, enabling specific non-covalent interactions known as chalcogen bonds (ChBs).^{16,17} This dual nature expands thiophene's potential for supramolecular chemistry applications.^{18,19} Given the depth of these σ -holes, sulfur typically forms weaker interactions than its heavier group 16 counterparts (with interaction strength in the order $\text{Te} > \text{Se} > \text{S} > \text{O}$). Moreover, sulfur in thiophene can participate in bifurcated contacts, where the atom interacts with multiple electron-rich sites. Both the size and magnitude of its σ -hole can be tuned by adjacent groups.²⁰ On the other hand, the aromatic features of thiophene offer a valuable platform for developing supramolecular scaffolds based on π electron

Microbiology, Bioorganic and Macromolecular Chemistry (MBMC) Unit, Faculty of Pharmacy, Université Libre de Bruxelles, 1050, Brussels, Belgium.
E-mail: franck.meyer@ulb.be

interactions,²¹ with its stacking properties being tunable through oxidation.^{22,23} These data demonstrate that this aromatic ring offers numerous opportunities in supramolecular chemistry, which can be further expanded through structural modifications with carefully selected atoms or functional groups. In recent years, the supramolecular toolbox has been enriched with a variety of non-covalent interactions, including the latest concepts based on σ -hole interactions, as detailed and compiled in a comprehensive review.²⁴

This highlight provides a concise overview of purpose-designed thiophenes and their diverse applications, illustrated with key examples from fields such as crystal engineering, solid-state synthesis, mechanochemistry, electronic materials, and biological sciences. The remarkable versatility of thiophene rings stems from their electron-rich core, which facilitates $\pi\cdots\pi$ interactions, and the sulfur atom, capable of acting as both an electron donor and a participant in chalcogen bonding. Functionalizing these rings with additional groups enables the formation of halogen (XB) and hydrogen bonds (HB) while fine-tuning $\pi\cdots\pi$ interactions. Key supramolecular features are illustrated with representative examples, primarily supported by available X-ray crystal structures, illustrating their roles in a variety of intra- and intermolecular interactions, including halogen, chalcogen, and hydrogen bonding, as well as $\pi\cdots\pi$ stacking. Where X-ray data are unavailable, complementary insights are provided through density functional theory (DFT) calculations and microscopy studies, further elucidating the structural and functional properties of these materials. For all figures presenting X-ray structures, colours are assigned as follows: C, grey; H, white; N, blue; F, yellow; S, orange; O, red; I, purple; Br, brown; Cl, green. Red dots represent the centre of aromatic rings or double bonds.

Halogen bonding

The halogen bond is a σ -hole-based interaction with characteristics similar to chalcogen bonds.^{25,26} The size and depth of the σ -hole, resulting from depopulation of the pz orbital, follow the trend $I > Br > Cl > F$, and can be further tuned by introducing electron-withdrawing groups near the halogen. Its magnitude can be estimated through molecular electrostatic potential (MEP) surface calculations, where the σ -hole corresponds to the region of maximum positive potential, denoted as $V_{S,max}$. A comparison of σ -hole values for elements from groups 16 and 17, as calculated by Bauzá and Frontera, is shown in Fig. 1.²⁷

Like chalcogen atoms, halogens can display dual behaviour, acting as both electron donors and acceptors.^{28,29} Over the past two decades, halogen bonds have been applied across a wide range of research fields, including crystal engineering,^{30,31} anion sensing,³² organic synthesis,³³ polymer chemistry,^{34,35} materials³⁶ and biological sciences.^{37,38}

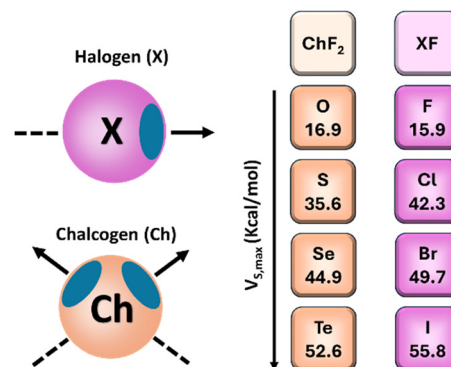


Fig. 1 Schematic representation of the σ -holes (blue regions) on halogen and chalcogen atoms (left), with their electrostatic potential $V_{S,max}$, calculated by Bauzá and Frontera at RI-MP2/def2-TZVP level of theory when connected to fluorine atoms (right).²⁷

Crystal engineering

To achieve the self-assembly of thiophene-based compounds *via* halogen bonding, various strategies involve incorporating halogen groups at the 2, 3, or 5 positions of the thiophene ring.

Recent studies highlighted the potential of these modified thiophenes as innovative building blocks in supramolecular chemistry considering their high interest in organic electronic.³⁹ As an example, 2,5-diiodothiophene (25DIT) was paired with a series of ditopic amines and onium salts to investigate its self-assembly behaviour. When combined with neutral amino groups like 4,4'-bipyridine (44BIPY), 25DIT formed one-dimensional chains in a 1:1 stoichiometric ratio, stabilized by $N\cdots I$ halogen bonds (Fig. 2). In contrast, co-crystallization with ammonium and phosphonium iodide or triiodide salts led to a variety of supramolecular architectures, spanning from zero- to two-dimensional structures. These assemblies were primarily stabilized by $I\cdots I^-$ or $I\cdots I_3^-$ interactions, with the complex containing trimethylbenzylammonium triiodide (NMe3BzI3) serving as an example of these interactions (Fig. 2). The study further suggested that these structural motifs could be tuned by adjusting the stoichiometry of the substituents (Fig. 2).⁴⁰

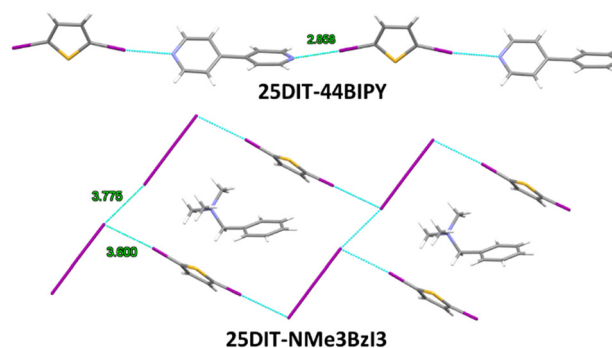


Fig. 2 X-ray structures of 25DIT-44BIPY and 25DIT-NMe3BzI3.

Additionally, a series of self-complementary 5-(4-pyridyl)-2-halothiophenes (with X = Cl (**PyClT**), Br (**PyBrT**), I (**PyIT**)) was investigated by DFT computation, ^1H NMR and X-ray crystallography (Fig. 3).

As expected, the σ -hole magnitude of halogen atom increases from Cl to Br to I, with $V_{\text{S,max}}$ values of 58, 80 and 113 kJ mol^{-1} , respectively, comparable to 1-iodoethynyl-4-iodobenzene (107 kJ mol^{-1}) but lower than 1,4-diiodotetrafluorobenzene ($>137 \text{ kJ mol}^{-1}$). In contrast, $V_{\text{S,min}}$ values of pyridyl nitrogen remain almost identical for all compounds. When **PyXT** compounds are combined with *N*-iodosuccinimide (NIS), $\text{N-I}\cdots\text{N}_{\text{Py}}$ interactions are favoured over $\text{N-I}\cdots\text{X-C}$ contacts, as highlighted by ^1H NMR spectroscopy.

Finally, X-ray structures of pure **PyXT** reveal linear organization governed by $\text{N}\cdots\text{X}$ halogen bonds.⁴¹ For thiophenes functionalized with an XB group at the 3-position, 3-((2,3,5,6-tetrafluoro-4-iodophenoxy)methyl)thiophene (**Thiol**) was tested with bipyridine ethane (**BiPyetha**), bipyridine ethylene (**BiPyethy**), and 4,4'-bipyridine (**44BIPY**).⁴² The **Thiol-BiPyetha** and **Thiol-BiPyethy** complexes formed trimeric systems through $\text{N}\cdots\text{I}$ halogen bonds, which were further organized into chains by weak $\text{S}\cdots\text{S}$ chalcogen interactions (Fig. 3).⁴³ Unexpectedly, the **Thiol-44BIPY** complex adopted a linear arrangement where both units alternated perfectly due to a unique combination of $\text{N}\cdots\text{I}$ halogen bonds and $\text{N}\cdots\text{S}$ chalcogen bonds (Fig. 3). According to DFT calculations, the chalcogen bond energy is approximately $-3.0 \text{ kcal mol}^{-1}$, significantly contributing to the crystal's cohesion.⁴⁴

By reversing the code, supramolecular scaffolds were also constructed using thiophene-based compounds incorporating

a pyridyl ring as the electron donor and iodoperfluorinated chains,⁴⁴ diiodoperfluoroarenes,⁴⁴ pentafluoroiodobenzene⁴⁵ or (iodoethynyl)benzene derivatives as halogen bond donors.^{46,47}

Solid-state polymerization

2,5-Dihalothiophene derivatives are frequently employed as monomers to synthesize corresponding polymers *via* solution-phase reactions.⁴⁸ Additionally, these compounds hold significant interest for the preparation of conductive materials through solid-state polymerization (SSP).⁴⁹ This process necessitates a highly ordered crystalline state of the monomeric precursors to facilitate polymerization. Early studies investigated the solid-state synthesis of conducting polythiophenes using 2,5-dihalo-3,4-ethylenedioxythiophenes (**DCEDOT**, **DBEDOT**, and **DIEDOT** with X = Cl, Br and I, respectively). Notably, **DBEDOT** can self-polymerize over an extended period (up to 2 years) or at moderate temperatures (50–80 $^{\circ}\text{C}$), whereas the iodinated derivative, **DIEDOT**, requires temperatures above 130 $^{\circ}\text{C}$, and the chlorinated analog, **DCEDOT**, remains unreactive. X-ray structures of **DBEDOT** reveal $\text{Br}\cdots\text{Br}$ contacts of type II in addition to $\text{S}\cdots\text{Br}$ and $\text{S}\cdots\text{S}$ chalcogen bonds. Similarly, **DCEDOT** and **DIEDOT** are mainly governed by $\text{X}\cdots\text{X}$ and $\text{S}\cdots\text{X}$ interactions

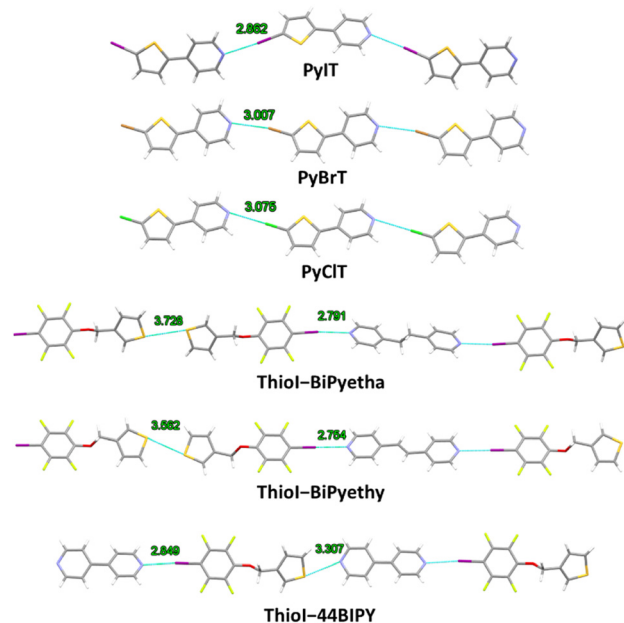


Fig. 3 X-ray structures of **PyClT**, **PyBrT**, **PyIT**, **Thiol-BiPyetha**, **Thiol-BiPyethy** and **Thiol-44BIPY**.

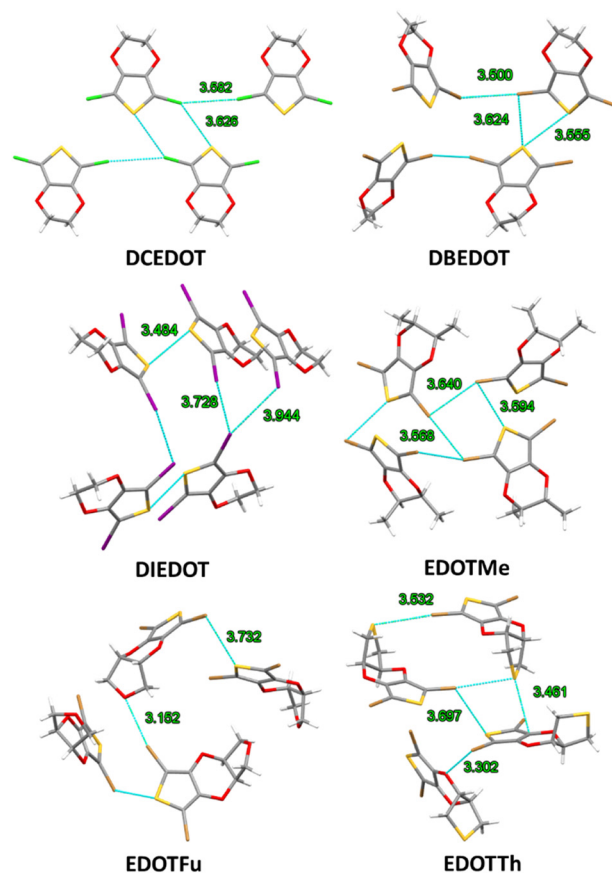


Fig. 4 X-ray structures of **DCEDOT**, **DBEDOT**, **DIEDOT**, **EDOTMe**, **EDOTFu** and **EDOTTh**.

(X = Cl, I) (Fig. 4).⁵⁰ Other studies have emphasized the importance of organizing units through X...X and π -stacking interactions to facilitate solid-state polymerization. The crystal packing of EDOT analogs, specifically **EDOTMe**, **EDOTFu** and **EDOTTh**, reveals distinct halogen bonding patterns: **EDOTMe** exhibits type II Br...Br halogen bonds, while **EDOTFu** and **EDOTTh** feature Br...O and Br...S interactions (Fig. 4). Furthermore, SSP reactivity follows the trend **EDOTMe** > **EDOTFu** ~ **EDOTTh**, which aligns with the less favourable molecular arrangements observed in **EDOTFu** and **EDOTTh**. Notably, the highest conductivity (4.2 S cm^{-1}) was achieved with the **EDOTMe**-based polymer. The authors suggest that X...X interactions may not be the primary factor driving SSP.⁵¹

Subsequent studies focused on a series of 2,5-dibromo-3-R-thiophenes (R = COONa, CN, CONH₂, CON(H)Me, CON(H)Bn, CON(CH₂CH₂)₂O, CON(H)NH₂, CON(H)OH), which formed chain, zigzag, and rhombic assemblies through Br...Br halogen bonds. Additional DFT calculations were conducted to correlate interaction strength with the SSP potential of these materials; however, the results for systems supported by Br...Br and I...I interactions appear inconsistent.⁵² On-surface synthesis using reactive metal-based substrates also offer an attractive approach for forming C–C bonds from halogenated compounds.⁵³ Utilizing this method, surface-assisted polymerization was carried out using 5,5''-dibromo-2,2':5',2''-terthiophene (**DBTT**) as a precursor to synthesize pure polythiophene *via* a dehalogenation Ullmann-type coupling reaction. Upon deposition on an Au(111) surface at room temperature, **DBTT** molecules self-assemble into triangular structures driven by Br...Br and Br...S interactions at low surface coverage and form closely packed motifs stabilized by Br...Br type I halogen bonds at high surface coverage (Fig. 5). Subsequent annealing initiates on-surface reactions, resulting in the formation of ordered polythiophene chains and cross-linked polymer networks.⁵⁴

Sensor

Conjugated macrocycles with well-defined shapes offer numerous advantages in organic electronics. They enhance intermolecular contacts and charge transport, exhibit unique optical and electronic properties, and can serve as hosts for target molecules, enabling various functional applications.⁵⁵ A cyclic, conjugated organic semiconductor was developed as an OFET sensing device, based on the combination of diphenyl perylene diimides (PDIs) and brominated bithiophenes (**PDI-BrBT**). The capsule-like structure self-assembled into thin films, driven by Br...PDI halogen bonds, a feature absent in the non-brominated analogue (**PDI-BT**) (Fig. 6). This halogen bonding enhanced the electron mobility of **PDI-BrBT** to approximately $1.5 \times 10^{-2} \text{ cm}^2 \text{ V}^{-1} \text{ s}^{-1}$, which is 20 times greater than that of **PDI-BT**. When exposed to chemical vapours, the hollow organic film responded with changes

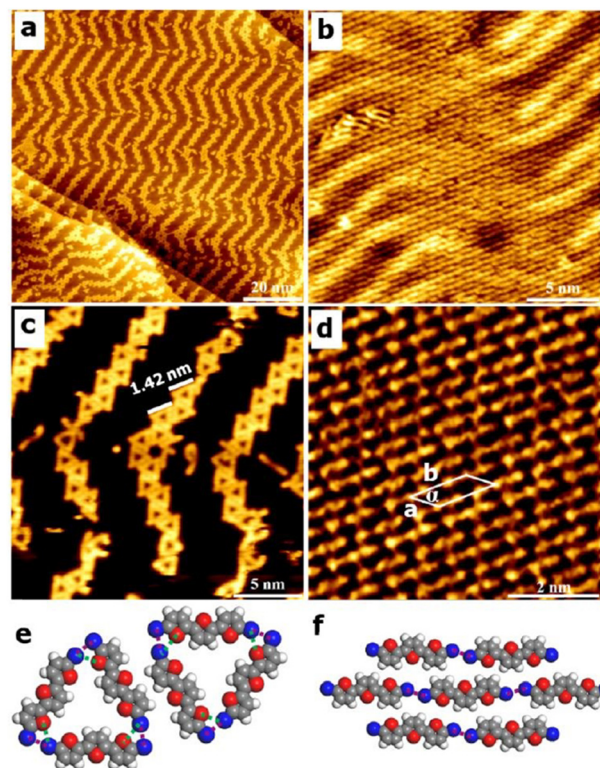


Fig. 5 (a) Large-scale and (c) high-resolution STM images showing triangle-like self-assembly after deposition of **DBTT** onto the Au(111) surface at room temperature with ~ 0.4 monolayer. (a) $V_s = 1000 \text{ mV}$, $I = 100 \text{ pA}$; (c) $V_s = -1000 \text{ mV}$, $I = 100 \text{ pA}$. (b) Large scale and (d) high-resolution STM images showing a close-packed self-assembly nanostructure of **DBTT** on the Au(111) substrate at room temperature with ~ 1.0 monolayer. $V_s = -600 \text{ mV}$, $I = 60 \text{ pA}$. (e and f) Proposed molecular models for the triangle-like and close-packed patterns. The dotted lines indicate the intermolecular interactions. One monolayer is defined as all the surface is covered by the ordered nanostructure (reproduced from ref. 54 with permission of the Royal Society of Chemistry).

in drain current. The cavity ($\sim 415 \text{ \AA}^3$) could accommodate a wide range of molecules, including ketones, alcohols, and nitriles, and even distinguish between hydrocarbons with similar structures, such as hexane, 1-hexyne, and 3-hexyne.⁵⁶

Mechanochemistry

In 2014, the self-assembly of complementary modified thiophenes—3-[(2,3,5,6-tetrafluoro-4-iodophenoxy)methyl]-thiophene (**ThioI**) and 4-(thiophen-3-ylmethoxy)pyridine (**ThioPy**)—yielded two polymorphic structures, **ThioI-ThioPyA** and **ThioI-ThioPyB**.

ThioI-ThioPyA exhibited both N...I halogen bonding and lone pair (lp)... π interactions, while **ThioI-ThioPyB** showed only halogen bonding (Fig. 6). Notably, the N...I bond distance in **ThioI-ThioPyA** (2.774 \AA) was shorter than that in **ThioI-ThioPyB** (2.830 \AA). DFT analysis confirmed the interplay between halogen bonds and lp... π contacts in these structures.⁵⁷ In recent years, mechanochemistry has

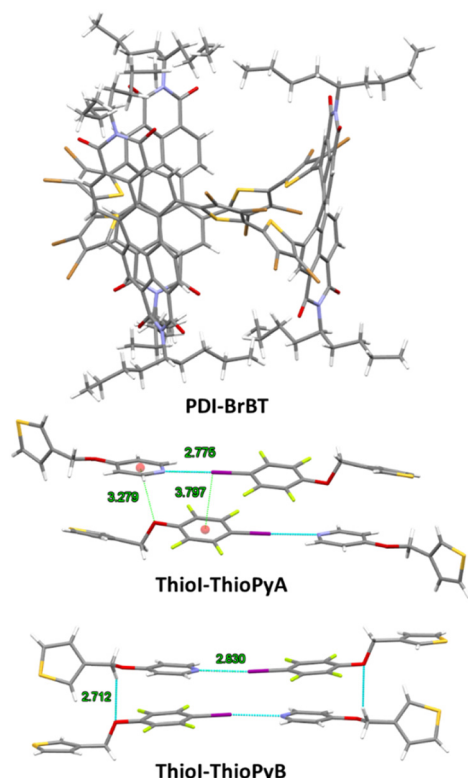


Fig. 6 X-ray structures of PDI-BrBT, Thiol-ThioPyA and Thiol-ThioPyB.

introduced new perspectives in synthetic chemistry, offering alternative pathways, innovative strategies, and significantly reducing solvent use.^{58,59} Considering these advantages, the formation of these polymorphs was further explored using mechanochemical methods, both in neat conditions and with liquid-assisted grinding (LAG) in THF, water, methanol, toluene, and dichloromethane. **ThioI-ThioPyA** formed under neat and methanol conditions, while **ThioI-ThioPyB** was obtained with the other solvents, indicating no direct correlation with solvent polarity or protic/aprotic character. Additionally, creating a supersaturated acetone suspension containing both forms led to a complete transformation of **ThioI-ThioPyB** into **ThioI-ThioPyA**, demonstrating that **ThioI-ThioPyA** is the thermodynamically stable form at this temperature and in this solvent environment.⁴⁴

It is worth noting that the iodination of 2,2'-bithiophene-5-carbaldehyde proceeded quantitatively by mechanoactivation using potassium dichloriodate monohydrate as reagent (Fig. 7) while the reaction works only in solution for 2,2'-bithiophene.⁶⁰

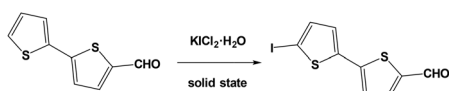


Fig. 7 Iodination of 2,2'-bithiophene-5-carbaldehyde by solid state reaction.

Chalcogen bonding

Inspired by the success and versatility of halogen bonds, researchers have increasingly focused on chalcogen bonds as a tool for molecular design. Although sulfur forms relatively weak CHBs, its applications in biological and material sciences have progressed significantly, often paralleling those of XB.⁶¹

Intramolecular interaction/conformational lock

One of the most attractive features of thiophene is its ability to form intramolecular interactions through its sulfur atom with various other atoms, thereby stabilizing specific molecular conformations. These interactions provide a foundation for diverse applications across fields such as molecular recognition, material design, and drug development.

Molecular balances. These intramolecular interactions have been utilized to investigate the nature of chalcogen bonds using synthetic molecular balances (**SMB**). These SMBs are designed with a (thio)formamide donor strategically placed near a thiophene (or selenophene) group, leveraging $O\cdots S$ and $S\cdots S$ interactions to uncover detailed bonding characteristics. Unlike hydrogen bonds, the independence of chalcogen bonds from solvent effects is unexpected and is more likely attributed to stabilizing $n \rightarrow \sigma^*$ orbital interactions, as determined by natural bond orbital (NBO) (Fig. 8).¹⁷

Organic electronic. Chalcogen bonds also play a pivotal role in the design of π -conjugated systems for organic electronics, where planarity and molecular packing are crucial for charge transport.⁶² For example, two thienyl-vinylene-based building blocks, **M1** and **M2** were compared to assess the role of intramolecular $S\cdots O$ interactions in

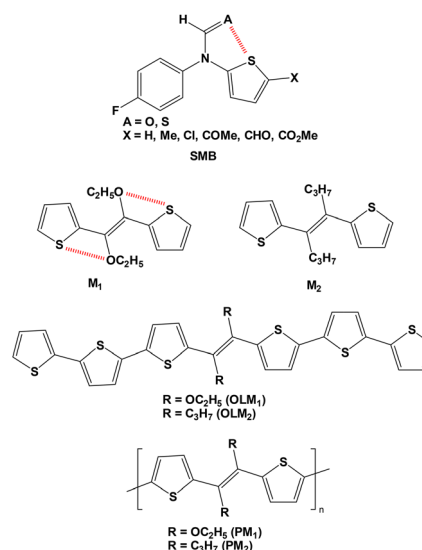


Fig. 8 Structures of synthetic molecular balances **SMB**, conjugated compounds **M1** and **M2**, and their respective derivatives: oligomers **OLM1** and **OLM2**, and homopolymers **PM1** and **PM2**.

determining their optoelectronic properties. X-ray crystallography revealed that **M1** contains an S...O interaction that locks its conformation, while **M2** lacks this feature, resulting in a reduced crystallinity and a twisted backbone, as indicated by DFT calculations. Cyclic voltammetry and optical spectroscopy further demonstrated that **M1** exhibits greater π -system delocalization compared to **M2**. As a result, the oligomer **OLM1** and homopolymer **PM1**, derived from **M1**, displayed hole mobilities of 3×10^{-3} and $3 \times 10^{-6} \text{ cm}^2 \text{ V}^{-1} \text{ s}^{-1}$, respectively. In comparison, both the oligomer **OLM2** and homopolymer **PM2** synthesized from **M2** were inactive in thin-film transistor applications (Fig. 8). These findings highlight the critical role of intramolecular interactions in promoting the formation of planar π -conjugated structures, thereby improving charge transport and enhancing overall material performance.⁶³

Furthermore, a broader investigation into small organic semiconductors highlighted correlations between the intramolecular interaction strength ($\text{X} \cdots \text{Y}$, where $\text{X} = \text{O}, \text{S}, \text{Se}, \text{Te}$ and $\text{Y} = \text{C}, \text{F}, \text{O}, \text{S}, \text{Cl}$), structural parameters, and optoelectronic properties. Significantly, interaction strength increases markedly in the order $\text{X} \cdots \text{F} < \text{X} \cdots \text{O}$ ($\text{X} = \text{S}, \text{Se}, \text{Te}$), with sulfur forming weaker chalcogen bonds compared to selenium and tellurium. Building on this understanding, A descriptor developed from this study provides a framework for predicting and tuning luminescence and charge transport properties. For example, the X-ray structure of a thiophene-based molecule, **PhMSO**, reveals a short S...O distance, effectively constraining the molecule's conformation (Fig. 9).⁶⁴

Drug design. Chalcogen bonding has also emerged as a valuable strategy in drug design.^{65,66} In 2018, a PDB survey identified over 6500 ligands containing sulfur or selenium atoms. Among these, more than 1500 S-containing and 20 Se-containing small-molecule ligands were found to interact with proteins through S/Se...X interactions, where X represents O, N, or S.⁶⁷ A novel series of microtubule polymerization inhibitors was designed based on the structure of 4-substituted methoxybenzoyl-aryl-thiazoles (SMART), incorporating a thiophene group to stabilize the molecule's conformation through intramolecular chalcogen bonding. This design was inspired by the structural features of drugs like acetazolamide and thiamethoxam (Fig. 10). DFT analysis of **TPO-7** confirms an intramolecular O...S



Fig. 9 X-ray structure of **PhMSO**.

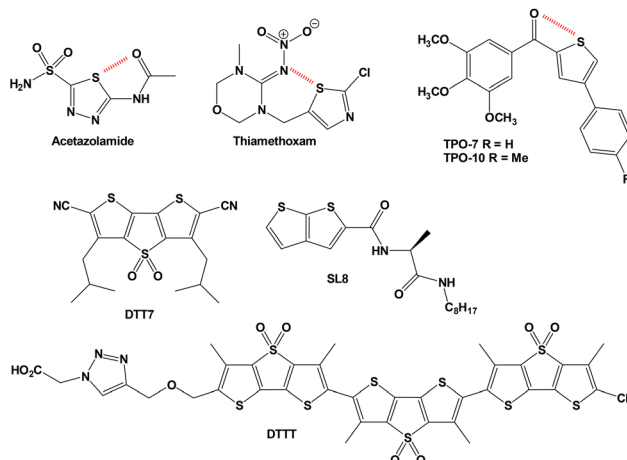


Fig. 10 Structures of acetazolamide, thiamethoxam, **TPO-7** and **TPO-10**, **DTT7**, **SL8** and **DTTT**.

interaction with an energy of $0.62 \text{ kcal mol}^{-1}$. *In vitro* antiproliferative assays against HCT-116 (human colonic carcinoma), MCF-7 (human breast carcinoma), and SGC-7901 (human gastric adenocarcinoma) cancer cell lines reveal IC₅₀ values as low as $0.023\text{--}0.133 \text{ }\mu\text{M}$ for **TPO-10** (Fig. 10). Molecular modelling further indicates that **TPO-10** is optimally positioned within the active site between the α and β tubulin subunits, suggesting it as a promising colchicine site inhibitor.⁶⁸

Transmembrane anion transport

Synthetic anion transporters are gaining significant attention due to their promising biological applications.⁶⁹ These systems are generally classified into two main categories: carriers and channels. In 2016, dithienothiophene-based receptors were explored as anion transporters through S...anion interactions using large unilamellar vesicles (LUVs) and the pH-sensitive fluorescent probe 8-hydroxy-1,3,6-pyrenetrisulfonate (HPTS). As halogen bond-based receptors, **DTT7** exhibited selectivity for chloride ions over oxoanions, with an effective concentration (EC₅₀) of $1.9 \text{ }\mu\text{M}$ (Fig. 10).⁷⁰ This design was further optimized by developing a **DTTT** trimer, which achieved enhanced transport activity with an EC₅₀ as low as $0.28 \text{ }\mu\text{M}$ (Fig. 10).⁷¹ Similarly, a bicyclic thiophene linked to the monopeptide **SL8** was employed to construct an anion channel (Fig. 10). Compared to previous scaffolds, **SL8** exhibits selectivity for perchlorate anion transport over Cl^- , Br^- , and NO_3^- anions by a factor of 4–8, achieving high transport efficiency with an EC₅₀ of $0.093 \text{ }\mu\text{M}$.⁷²

Supramolecular helices

Helical structures, ubiquitous in nature, are fundamental to complex biological systems, inspiring scientists to develop synthetic helical materials.

Harnessing supramolecular interactions, these engineered helices promise to advance materials science and deepen our

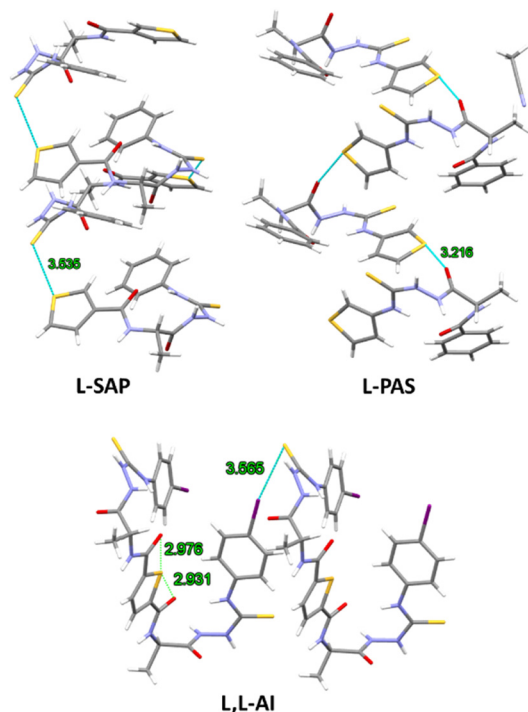


Fig. 11 X-ray structures of L-SAP, L-PAS and L,L-AI.

understanding of biological processes.⁷³ In this context, researchers have explored thiophene-based systems to investigate supramolecular helices formed through chalcogen bonds. Thiophene moieties were appended to the N-terminus (**L-SAP**) or C-terminus (**L-PAS**) of an alanine-based azapeptides containing a β -turn structure to investigate the potential formation of supramolecular helices *via* chalcogen bonds (Fig. 11). It appears that **L-SAP** forms a left-handed (M)-helix through intermolecular S \cdots S chalcogen bonding between sulfur atoms of the thiophene and thiourea groups. In contrast, **L-PAS** forms a right-handed (P)-helix, driven by intermolecular S \cdots O chalcogen bonding between the thiophene and amidinothiourea moieties.⁷⁴ Another approach involved introducing a 2,5-thiophenediamide group into the symmetric azapeptide **L,L-AI**, enabling intramolecular S \cdots O chalcogen bonding. This modified peptide, which adopts a β -turn structure in a *cis*-conformation, self-assembles into a single-stranded supramolecular helix, stabilized further by intermolecular S \cdots I halogen bonding due to iodoaryl groups at both termini (Fig. 11). Circular dichroism analysis indicates that **L,L-AI** retains a similar structure in solution (CH₃CN) as in the solid state, with thermal stability up to at least 70 °C.⁷⁵

Hydrogen bonding

Fluorescence

Oligothiophenes are of great interest across diverse research areas, including organic semiconductors and fluorescent markers for biological systems.

Their unique optical and electronic properties, which can be fine-tuned through structural modifications, make them valuable in material design and biosensors.^{76,77}

Two terthiophene derivatives, namely 5,5''-dimethyl-2,2':5',2''-terthiophene (**DM3T**) and (5,5''-dimethyl-[2,2':5',2''-terthiophen]-3'-yl)methanol (**DM3TMeOH**) were co-crystallized with dipyrindine (**44BiPy**) with the initial aim of promoting chalcogen bonding interactions between the nitrogen atoms of **44BiPy** and the sulfur atoms in the terthiophene core. However, the resulting supramolecular structures revealed unexpected interactions and organization. The supramolecular structure of **DM3T-44BiPy** formed separate, infinite layers of both units. Interestingly, instead of the targeted chalcogen bonding, the layers were stabilized solely by weak C-H \cdots π interactions, demonstrating the dominance of alternative non-covalent forces in this assembly. In the case of **DM3TMeOH-44BiPy**, a cyclic arrangement involving four molecules was observed, with the O-H \cdots N and C-H \cdots N hydrogen bonds playing a key role in stabilizing this structure (Fig. 12). Fluorescence spectroscopy revealed emission colours under UV light (365 nm) for **DM3T** and **DM3TMeOH** in solution and solid states. Adding **44BiPy** caused fluorescence quenching, more pronounced in the solid state for **DM3T-44BiPy** and **DM3TMeOH-44BiPy** (Fig. 13).⁷⁸

[2 + 2] photocycloaddition

The [2 + 2] photocyclization in the solid state provides an environmentally friendly method to form covalent bonds with high regio- and stereoselectivity. Geometrically, successful photocyclization requires compliance with Schmidt's topochemical postulate, which specifies that olefinic bonds must be parallel and separated by less than 4.2 Å.⁷⁹ The main

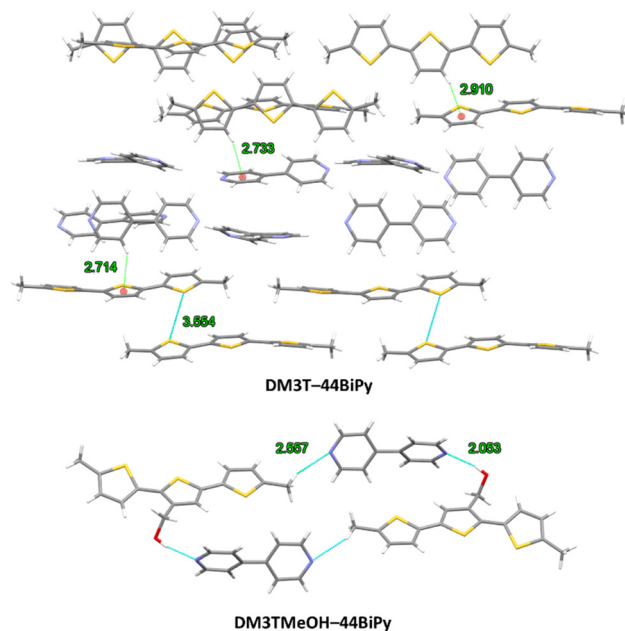


Fig. 12 X-ray structures of **DM3T-44BiPy** and **DM3TMeOH-44BiPy**.

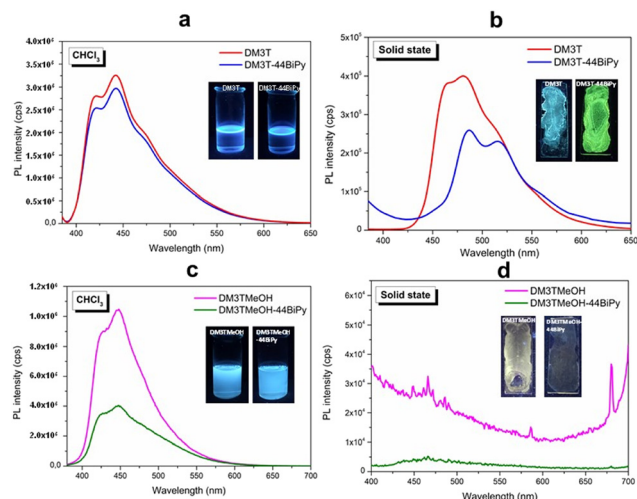


Fig. 13 Room-temperature fluorescence spectra of DM3T and DM3T-44BiPy in (a) CHCl₃ solution and (b) drop-cast thin film. Fluorescence of DM3TMeOH and DM3TMeOH-44BiPy in (c) CHCl₃ solution and (d) drop-cast thin film (reproduced from ref. 78 with permission of MDPI).

challenge lies in arranging molecules through crystal engineering strategies to position the double bonds in a way that satisfies these spatial requirements. In 2014, the photodimerization of *trans*-1-(4-pyridyl)-2-(3-thienyl)ethylene (β -PTE) was explored, as thiophene-based cycloadducts are rare, and this approach offers a high degree of regiocontrol. Pure β -PTE adopts an edge-to-face packing, so 4,6-diiodoresorcinol (4,6-diI-res) and 4,6-dichlororesorcinol (4,6-diCl-res) were employed as templates to align β -PTE in a face-to-face π -stacked arrangement.

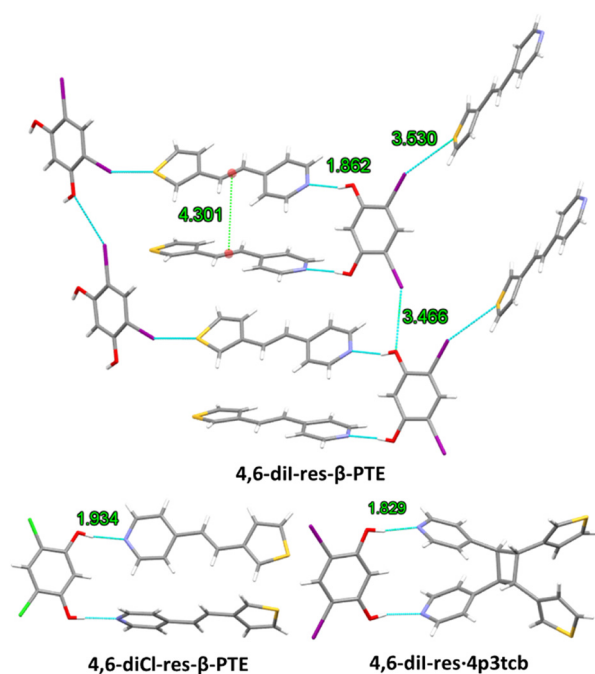


Fig. 14 X-ray structures of 4,6-diI-res- β -PTE; 4,6-diCl-res- β -PTE and 4,6-diI-res-4p3tcb.

While the hydrogen-bonded 4,6-diCl-res- β -PTE complex retained an edge-to-face packing, 4,6-diI-res- β -PTE achieved the required face-to-face orientation, with C=C centroid-centroid distances between 4.147 and 4.301 Å. Additionally, weak O \cdots I and S \cdots I halogen bonds stabilize the structure.⁸⁰ After 100 hours of UV irradiation, the styrylthiophene underwent a [2 + 2] photocycloaddition to give the cycloadduct 4p3tcb, confirmed by ¹H NMR and single-crystal X-ray diffraction (Fig. 14).⁸¹

Solar cell performance

As previously mentioned, designing high-performance semiconductor polymers effectively involves creating a highly planar polymer backbone with extended π -electron delocalization, which reduces the energy band gap and strengthens inter-chain $\pi\cdots\pi$ interactions. Early methods achieved this by covalently linking aromatic rings to restrict single-bond rotation. To achieve this, two thiophene-pyrazine-thiophene building blocks with carbamate (TPTCA) or carboxamide (TPTCX) groups at the 3-position were designed.

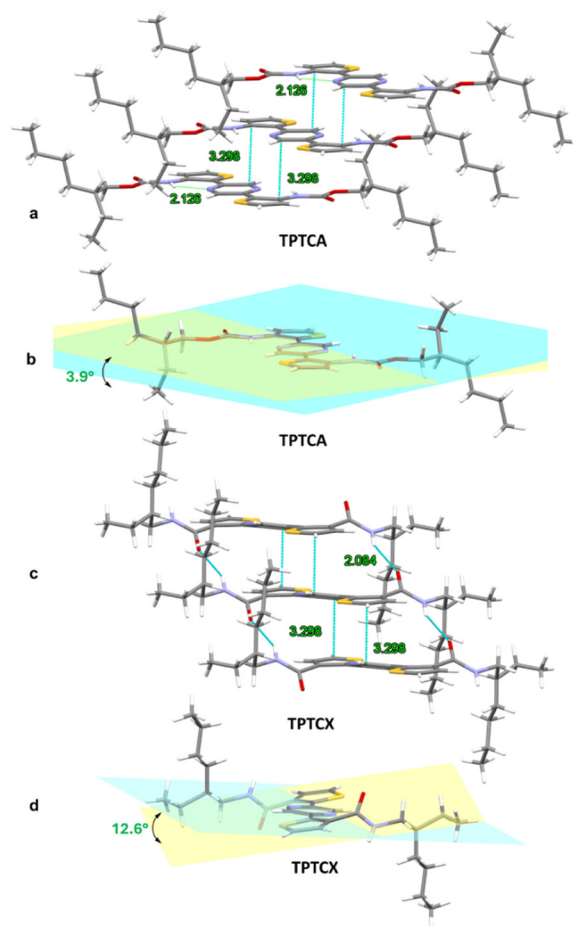


Fig. 15 X-ray structures of TPTCA (a and b) and TPTCX (c and d) highlighting the π - π stacking (a and c) and the dihedral angle made by the thiophene and pyrazine rings (b and d).

The X-ray structure of **TPTCA** reveals two intramolecular N \cdots H hydrogen bonds that lock the conformation into an almost coplanar arrangement (dihedral angle $\sim 4^\circ$), enhancing π -electron delocalization (Fig. 15). In contrast, **TPTCX** forms intermolecular N \cdots H hydrogen bonds involving the amide groups, resulting in a less planar structure with a dihedral angle of $\sim 13^\circ$ (Fig. 15). Three polymers incorporating **TPTCX** or **TPTCA** units were synthesized, and their photovoltaic properties were evaluated. The **TPTCA**-based compounds, **PCAA** and **PCAb**, achieved power conversion efficiencies (PCE) of 5.2% and 7.9%, respectively, while the **TPTCX**-based compound, **PCX**, had a PCE of only 0.1% (Fig. 16, Table 1).

Two-dimensional grazing incidence wide-angle X-ray scattering (2D-GIWAXS) analysis revealed that polymers with carbamate side chains provided tighter interchain packing in blend films compared to those with carboxamide side chains, facilitating charge transport and contributing to improved short-circuit current density (J_{sc}) and fill factor (FF).⁸²

A recent review highlights the strategic use of hydrogen bonding, alongside a wide variety of functional groups, to tailor the diverse physicochemical properties of conjugated polymers.⁸³

Non-linear optic (NLO)

Second harmonic generation (SHG) and nonlinear optical (NLO) properties are essential in optical data storage and laser technologies. Noncentrosymmetric SHG organic compounds are often designed with electron-rich and electron-deficient groups bridged by π -conjugated structures, offering high NLO coefficients, rapid response times, and design flexibility.

Two thiophene derivatives, **TM1** and **TM2**, were developed with an ammonium HB donor group at one chain end and

Table 1 Photovoltaic parameters of the OPV devices using **Y6** as small molecular acceptor

Device	V_{oc} (V)	J_{sc} (mA cm ⁻²)	FF (%)	PCE (%)
PCX:Y6	0.62 (± 0.01)	0.5 (± 0.1)	23.4 (± 0.2)	0.1 (± 0.001)
PCAA:Y6	0.83 (± 0.01)	12.8 (± 0.2)	48.9 (± 0.5)	5.2 (± 0.2)
PCAb:Y6	0.83 (± 0.01)	18.1 (± 0.4)	52.3 (± 0.3)	7.9 (± 0.2)

either a pyridyl (**TM1**) or pyridinium (**TM2**) electron-deficient group. **TM1** achieves a non-centrosymmetric structure due to pyridyl \cdots H interactions (Fig. 17), yielding an SHG response three times higher than the inorganic potassium dihydrogen phosphate (KDP) crystal reference, along with excellent optical transparency and stability. In contrast, **TM2** exhibits inversion symmetry and no SHG signal (Fig. 17).⁸⁴

π - π interactions

Semiconductor

In 2003, new n-type thiophene-based organic semiconductors were developed by introducing electron-deficient perfluoroarene groups to p-type oligothiophene cores. This modification was intended to lower LUMO energies for improved electron injection, adjust steric interactions to influence orbital energies, and place fluoroarene moieties centrally to maintain a rodlike structure. X-ray crystallography showed that quaterthiophene (**5,5''QT**) and bis-dithiophene (**5,5'BDT**) possess planar cores, whereas bis-dithiophenyl (**4,4'BOF**) has a large torsional angle (53.9°) between adjacent fluoroarene rings, disrupting π conjugation (Fig. 18). Due to $\pi\cdots\pi$ stacking and F \cdots F contacts, **5,5''QT** forms slipped-packed chains, and **5,5'BDT** adopts a zig-zag arrangement. The same interactions also appear in **4,4'BOF**. Electrical measurements indicate that **5,5''QT** behaves as an n-type semiconductor, while **5,5'BDT** and **4,4'BOF** are p-type, with carrier mobilities (μ in cm² V⁻¹ s⁻¹) as follows: **5,5''QT** (0.08) > **5,5'BDT** (0.01) \gg **4,4'BOF** (4×10^{-5}). This trend is attributed to the microstructural organization, as the planar and closely $\pi\cdots\pi$ stacked structures of **5,5''QT** and **5,5'BDT**

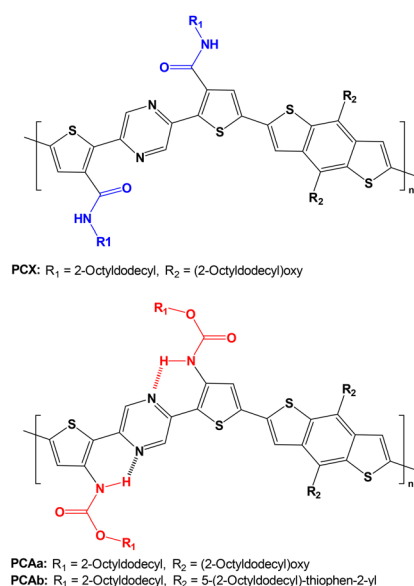


Fig. 16 Structures of polymers **PCX**, **PCAA** and **PCAb**.

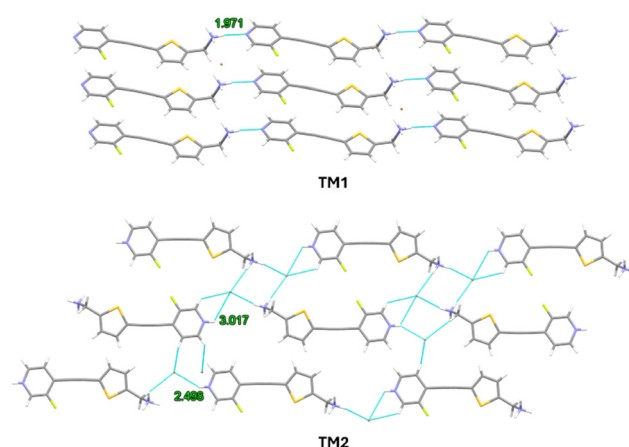


Fig. 17 X-ray structures of **TM1** (top) and **TM2** (bottom).

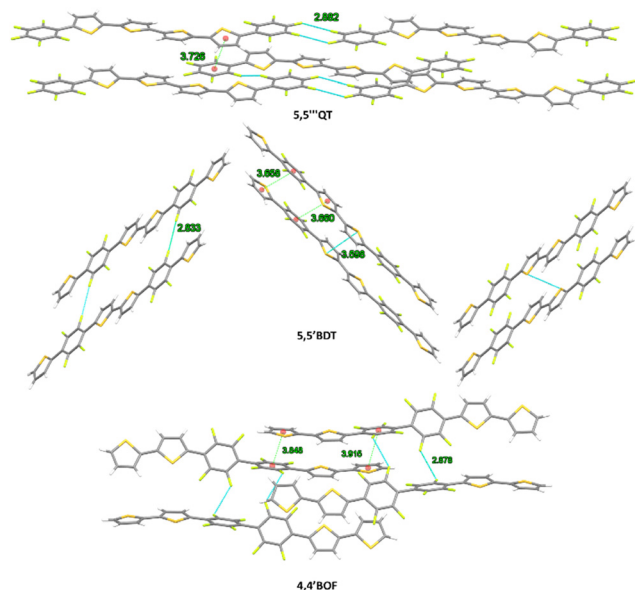


Fig. 18 X-ray structures of 5,5''QT, 5,5'BDT and 4,4'BOF.

favour in-plane charge transport, unlike the poorly conjugated 4,4'BOF.⁸⁵

Polymer organization

The supramolecular organization of (*E*)-2,5-dibromo-3-styrylthiophene (3ST) and (*E*)-2,5-dibromo-3-(2-(perfluorophenyl) vinyl)thiophene (3STF), was investigated to evaluate their ability to organize conducting polymeric chains. 3ST formed a columnar arrangement in a head-to-head mode, driven by $\pi \cdots \pi$ interactions with centroid-to-centroid distances of 3.942 Å, resulting in an unusual non-centrosymmetric organization

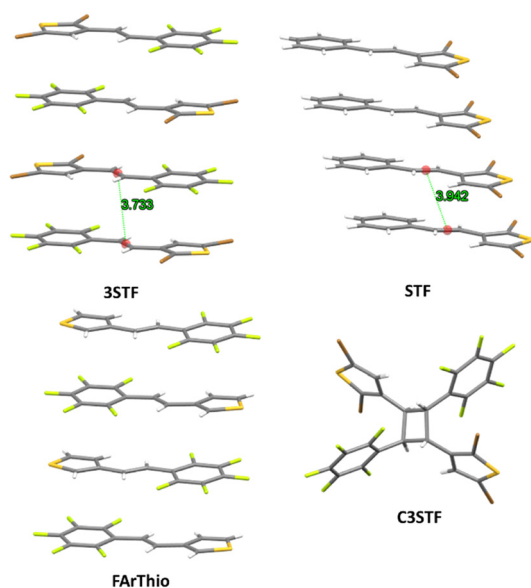


Fig. 19 X-ray structures of 3STF, STF, FarThio, and C3STF.

(Fig. 19). In contrast, 3STF exhibited a similar columnar order in a head-to-tail fashion, with distances of 3.646 Å within pairs and 3.733 Å between pairs. This arrangement resembles that of (*E*)-3-(2,3,4,5,6-pentafluorostyryl)-thiophene (FarThio).⁸⁶ These short distances facilitated a [2 + 2] photocycloaddition upon UV light irradiation (340 nm) for 24 hours, leading to the formation of a cyclobutane derivative C3STF (Fig. 19). Building on this, two diblock copolymers—poly(3-hexylthiophene)-*b*-poly(3-styrylthiophene) (P3HT-*b*-P3ST) and poly(3-hexylthiophene)-*b*-poly(3-(2',3',4',5',6'-pentafluorostyryl)thiophene) (P3HT-*b*-P3STF)—were synthesized and subjected to the same irradiation conditions. The resulting ¹H NMR spectra showed new signals corresponding to cyclobutane protons, confirming the successful [2 + 2] photocycloaddition and the remarkable alignment of the oligomeric chains.⁸⁷

Drug design

Interactions between aromatic groups are essential for the architecture of biomolecules, including DNA and protein folding, as well as the stabilization of protein–ligand complexes.⁸⁸ These interactions rank as the third most common type in protein–ligand binding and can occur in distinct geometries, such as edge-to-face or face-to-face arrangements.⁸⁹ *Orthoebolavirus zairensis* (EBOV), the causative agent of Ebola virus disease, encodes several viral proteins, including the EBOV glycoprotein (EBOV-GP), which facilitates viral entry into host cells.⁹⁰ EBOV-GP interacts with the Niemann-Pick C1 (NPC1) cholesterol transporter to release the viral genome into the cytoplasm. To disrupt this critical interaction and inhibit viral entry, a series of ligands

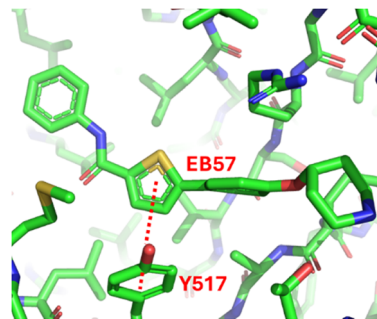
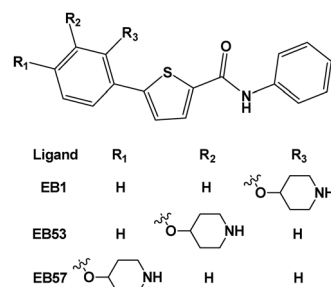


Fig. 20 Structures of ligands EB1, EB53 and EB57 (top). Representative binding mode of EB57 and tyrosine residue Y517 (bottom). Colours are as follows: C, green; S, orange; O, red; N, blue.

based on the thiophene hit compound **EB1** were designed (Fig. 20). Among these, compounds **EB53** and **EB57** showed potent antiviral activity, with EC₅₀ values of 0.30 μ M and 0.19 μ M, respectively, against replicative EBOV. The mode of action of these inhibitors was elucidated through docking studies and molecular dynamics (MD) simulations, employing the protein-toremifene crystal structure (PDB: 5JQ7) as a template. The results revealed that the thiophene ring forms a crucial $\pi\cdots\pi$ stacking interaction with tyrosine residue Y517 in the glycoprotein, a key interaction that stabilizes the inhibitor binding and disrupts the NPC1/EBOV-GP interaction (Fig. 20). Furthermore, **EB57** exhibited favourable characteristics, including robust metabolic stability, a lack of cardiotoxicity, and the ability to cross the blood–brain barrier.⁹¹

Conclusions

Thiophene, a versatile and ubiquitous heterocycle, continues to play a pivotal role across diverse scientific domains due to its unique electronic properties, structural flexibility, and ability to engage in various supramolecular interactions. Its inherent characteristics enable a wide range of non-covalent interactions, such as chalcogen bonding and $\pi\cdots\pi$ stacking. The functionalization of thiophene rings with tailored substituents, including group 17 elements, has further enhanced their supramolecular versatility, enabling the design of advanced materials with precise and innovative functionalities.

In materials science, thiophene derivatives have been instrumental in developing high-performance organic semiconductors, solar cells, sensors, and other electronic devices. By carefully designing molecular structures and leveraging supramolecular interactions, researchers have significantly improved the performance and efficiency of these devices. In medicinal chemistry, some thiophene-based compounds show potential for optimizing drug efficacy through their ability to fine-tune molecular properties. Additionally, modified-thiophenes are being explored for their potential in facilitating transmembrane anion transport and serving as organized building blocks for subsequent solid-state reactions.

Crystallographic studies, complemented by microscopy and density functional theory (DFT) analyses, have been crucial in unravelling the structure–property relationships of thiophene derivatives. As the field progresses, the integration of supramolecular principles with thiophene chemistry holds immense promise for addressing contemporary challenges in energy, health, and sustainability. For instance, incorporating halogen bond donor groups into thiophene derivatives offers new avenues for achieving sub-nanoscale structural precision in the supramolecular organization of polythiophenes. Such control over molecular arrangement can enhance the properties of functional materials.⁹² Additionally, halogen-bond-driven strategies can facilitate the formation of nanocomposites with carbon nanotubes,^{93,94} enabling the

development of advanced materials for applications in electrochemical sensing and battery electrodes, where performance and efficiency are critical.^{95,96} Cyclobutane derivatives offer intriguing building blocks for constructing unconventional architectures with unique functional properties.^{97,98} Notably, these compounds can serve as templates for the formation of porous systems, which hold great promise in a variety of applications, including advanced electrode materials for energy storage and efficient systems for detecting and removing pollutants or contaminants from the environment.^{99,100} By exploring new analogues, such as oligothiophenes, fused rings, and heterocycles incorporating other group 16 elements, researchers are paving the way for transformative advancements in crystal engineering, materials science, and beyond.

Data availability

There is no data supporting this article.

Conflicts of interest

There are no conflicts to declare.

Acknowledgements

AST acknowledges FNRS for postdoctoral fellowship (Grant Agreement PDR 35275398).

Notes and references

- 1 R. Shah and P. K. Verma, *BMC Chem.*, 2019, **13**, 54.
- 2 A. Mori, *Bull. Chem. Soc. Jpn.*, 2020, **93**, 1200–1212.
- 3 L. Björk, T. Klingstedt and K. P. R. Nilsson, *ChemBioChem*, 2023, **24**, e202300044.
- 4 G. Turkoglu, M. E. Cinar and T. Ozturk, *Top. Curr. Chem.*, 2017, **375**, 84.
- 5 F. Di Maria, M. Zangoli and G. Barbarella, *Org. Mater.*, 2021, **3**, 321–336.
- 6 F. Meyer, *Prog. Polym. Sci.*, 2015, **47**, 70–91.
- 7 S. R. M. Ibrahim, H. M. Abdallah, A. M. El-Halawany and G. A. Mohamed, *Phytochem. Rev.*, 2016, **15**, 197–220.
- 8 S. R. M. Ibrahim, A. M. Omar, A. A. Bagalagel, R. M. Diri, A. O. Noor, D. M. Almasri, S. G. A. Mohamed and G. A. Mohamed, *Plants*, 2022, **11**, 539.
- 9 A. L. Souto, M. Sylvestre, E. D. Tölke, J. F. Tavares, J. M. Barbosa-Filho and G. Cebrián-Torrejón, *Molecules*, 2021, **26**, 4835.
- 10 H. Wu, X. Lu, J. Xu, X. Zhang, Z. Li, X. Yang and Y. Ling, *Molecules*, 2022, **27**, 8700.
- 11 R. Shah and P. K. Verma, *Chem. Cent. J.*, 2018, **12**, 1–22.
- 12 S. Pathania, R. K. Narang and R. K. Rawal, *Eur. J. Med. Chem.*, 2019, **180**, 486–508.
- 13 Archana, S. Pathania and P. A. Chawla, *Bioorg. Chem.*, 2020, **101**, 104026.
- 14 I. E. Palamà, G. Maiorano, G. Barbarella and G. Gigli, *Nano Sel.*, 2023, **4**, 463–485.

- 15 G. Barbarella, A. Capodilupo, C. Bettini and G. Gigli, *Phosphorus, Sulfur Silicon Relat. Elem.*, 2011, **186**, 1074–1084.
- 16 L. Vogel, P. Wonner and S. M. Huber, *Angew. Chem., Int. Ed.*, 2019, **58**, 1880–1891.
- 17 D. J. Pascoe, K. B. Ling and S. L. Cockroft, *J. Am. Chem. Soc.*, 2017, **139**, 15160–15167.
- 18 J. S. Murray, P. Lane, T. Clark and P. Politzer, *J. Mol. Model.*, 2007, **13**, 1033–1038.
- 19 C. B. Aakeroy, D. L. Bryce, G. R. Desiraju, A. Frontera, A. C. Legon, F. Nicotra, K. Rissanen, S. Scheiner, G. Terraneo, P. Metrangolo and G. Resnati, *Pure Appl. Chem.*, 2019, **91**, 1889–1892.
- 20 A. Dhaka, I. R. Jeon and M. Fourmigué, *Acc. Chem. Res.*, 2024, **57**, 362–374.
- 21 T. Mori, *CrystEngComm*, 2023, **25**, 6266–6278.
- 22 D. A. Scherlis and N. Marzari, *J. Am. Chem. Soc.*, 2005, **127**, 3207–3212.
- 23 F. Rodríguez-Ropero, J. Casanovas, D. Zanuy and C. Alemán, *Chem. Phys. Lett.*, 2010, **488**, 177–181.
- 24 L. Brammer, A. Peuronen and T. M. Roseveare, *Acta Crystallogr., Sect. C: Struct. Chem.*, 2023, **79**, 204–216.
- 25 G. Cavallo, P. Metrangolo, R. Milani, T. Pilati, A. Priimagi, G. Resnati and G. Terraneo, *Chem. Rev.*, 2016, **116**, 2478–2601.
- 26 L. C. Gilday, S. W. Robinson, T. A. Barendt, M. J. Langton, B. R. Mullaney and P. D. Beer, *Chem. Rev.*, 2015, **115**, 7118–7195.
- 27 A. Bauzá and A. Frontera, in *Supramolecular Assemblies Based on Electrostatic Interactions*, ed. M. A. Aboudzadeh and A. Frontera, Springer International Publishing, Cham, 2022, pp. 203–241.
- 28 G. Berger, K. Robeyns, J. Soubhye, R. Wintjens and F. Meyer, *CrystEngComm*, 2016, **18**, 683–690.
- 29 G. Berger, J. Soubhye, A. van der Lee, C. Vande Velde, R. Wintjens, P. Dubois, S. Clément and F. Meyer, *ChemPlusChem*, 2014, **79**, 552–558.
- 30 G. Gattuso, R. Liantonio, P. Metrangolo, F. Meyer, A. Pappalardo, M. F. Parisi, T. Pilati, I. Pisagatti and G. Resnati, *Supramol. Chem.*, 2006, **18**, 235–243.
- 31 V. Kumar, T. Pilati, G. Terraneo, F. Meyer, P. Metrangolo and G. Resnati, *Chem. Sci.*, 2017, **8**, 1801–1810.
- 32 A. Brown and P. D. Beer, *Chem. Commun.*, 2016, **52**, 8645–8658.
- 33 R. L. Sutar and S. M. Huber, *ACS Catal.*, 2019, **9**, 9622–9639.
- 34 G. Berger, J. Soubhye and F. Meyer, *Polym. Chem.*, 2015, **6**, 3559–3580.
- 35 P. Frangville, A. S. Tanwar, S. Kumar, M. Gelbcke, N. Wauthoz, S. Basov, M. J. Van Bael, K. Van Hecke and F. Meyer, *Mater. Today Chem.*, 2024, **40**, 102234.
- 36 G. Berger, P. Frangville and F. Meyer, *Chem. Commun.*, 2020, **56**, 4970–4981.
- 37 R. Wilcken, M. O. Zimmermann, A. Lange, A. C. Joerger and F. M. Boeckler, *J. Med. Chem.*, 2013, **56**, 1363–1388.
- 38 R. S. Czarny, A. N. Ho and P. S. Ho, *Chem. Rec.*, 2021, **21**, 1240–1251.
- 39 A.-L. Barrès, M. Allain, P. Frère and P. Batail, *Isr. J. Chem.*, 2014, **54**, 689–698.
- 40 A. C. Ragusa, A. J. Peloquin, C. D. McMillen and W. T. Pennington, *Cryst. Growth Des.*, 2022, **22**, 1906–1913.
- 41 A. Koivuporras, A. Mailman, H. Guo, A. Priimagi and R. Puttreddy, *Cryst. Growth Des.*, 2023, **23**, 8889–8896.
- 42 M. Baldrigi, P. Metrangolo, F. Meyer, T. Pilati, D. Proserpio, G. Resnati and G. Terraneo, *J. Fluorine Chem.*, 2010, **131**, 1218–1224.
- 43 S. Scheiner, *J. Phys. Chem. A*, 2022, **126**, 4025–4035.
- 44 S. Kumar, C. Body, T. Leyssens, K. Van Hecke, G. Berger, A. Van der Lee, D. Laurencin, S. Richeter, S. Clément and F. Meyer, *Cryst. Growth Des.*, 2023, **23**, 2442–2454.
- 45 I. Hammer, G. S. Tschumper and D. L. Watkins, *RSC Adv.*, 2015, **5**, 82544–82548.
- 46 S. T. Nguyen, A. L. Rheingold, G. S. Tschumper and D. L. Watkins, *Cryst. Growth Des.*, 2016, **16**, 6648–6653.
- 47 S. N. Johnson, T. L. Ellington, D. T. Ngo, J. L. Nevarez, N. Sparks, A. L. Rheingold, D. L. Watkins and G. S. Tschumper, *CrystEngComm*, 2019, **21**, 3151–3157.
- 48 B. Amna, H. M. Siddiqi, A. Hassan and T. Ozturk, *RSC Adv.*, 2020, **10**, 4322–4396.
- 49 J. W. Lauher, F. W. Fowler and N. S. Goroff, *Acc. Chem. Res.*, 2008, **41**, 1215–1229.
- 50 H. Meng, D. F. Perepichka, M. Bendikov, F. Wudl, G. Z. Pan, W. Yu, W. Dong and S. Brown, *J. Am. Chem. Soc.*, 2003, **125**, 15151–15162.
- 51 M. Lepeltier, J. Hiltz, T. Lockwood, F. Bélanger-Gariépy and D. F. Perepichka, *J. Mater. Chem.*, 2009, **19**, 5167–5174.
- 52 S. V. Baykov, S. I. Presnukhina, A. S. Novikov, A. A. Shetnev, V. P. Boyarskiy and V. Y. Kukushkin, *Cryst. Growth Des.*, 2021, **21**, 2526–2540.
- 53 Q. Shen, H. Y. Gao and H. Fuchs, *Nano Today*, 2017, **13**, 77–96.
- 54 L. Liu, X. Miao, T. Shi, X. Liu, H. L. Yip, W. Deng and Y. Cao, *Nanoscale*, 2020, **12**, 18096–18105.
- 55 M. Iyoda, J. Yamakawa and M. J. Rahman, *Angew. Chem., Int. Ed.*, 2011, **50**, 10522–10553.
- 56 B. Zhang, R. Hernández Sánchez, Y. Zhong, M. Ball, M. W. Terban, D. Paley, S. J. L. Billinge, F. Ng, M. L. Steigerwald and C. Nuckolls, *Nat. Commun.*, 2018, **9**, 1957.
- 57 G. Berger, J. Soubhye, A. Van Der Lee, C. Vande Velde, R. Wintjens, P. Dubois, S. Clément and F. Meyer, *ChemPlusChem*, 2014, **79**, 552–558.
- 58 F. Cuccu, L. De Luca, F. Delogu, E. Colacino, N. Solin, R. Mocchi and A. Porcheddu, *ChemSusChem*, 2022, **15**, e202200362.
- 59 J. L. Do and T. Frišćić, *ACS Cent. Sci.*, 2017, **3**, 13–19.
- 60 G. Sereda, A. M. Sarkar, A. Hussain and N. Zefirov, *Synthesis*, 2020, **52**, 1140–1146.
- 61 K. T. Mahmudov, M. N. Kopylovich, M. F. C. Guedes Da Silva and A. J. L. Pombeiro, *Dalton Trans.*, 2017, **46**, 10121–10138.

- 62 J. Roncali, P. Blanchard and P. Frère, *J. Mater. Chem.*, 2005, **15**, 1589–1610.
- 63 H. Huang, Z. Chen, R. P. Ortiz, C. Newman, H. Usta, S. Lou, J. Youn, Y. Y. Noh, K. J. Baeg, L. X. Chen, A. Facchetti and T. Marks, *J. Am. Chem. Soc.*, 2012, **134**, 10966–10973.
- 64 M. Liu, X. Han, H. Chen, Q. Peng and H. Huang, *Nat. Commun.*, 2023, **14**, 2500.
- 65 S. Jena, J. Dutta, K. D. Tulsian, A. K. Sahu, S. S. Choudhury and H. S. Biswal, *Chem. Soc. Rev.*, 2022, **51**, 4261–4286.
- 66 M. R. Koebel, A. Cooper, G. Schmadeke, S. Jeon, M. Narayan and S. Sirimulla, *J. Chem. Inf. Model.*, 2016, **56**, 2298–2309.
- 67 K. Kristian, J. Fanfrlík and M. Lepšík, *ChemPhysChem*, 2018, **19**, 2540–2548.
- 68 L. Li, Z. Zou, B. Xue, B. Pang, Y. Yang, Q. Guan, B. Li and W. Zhang, *Biochem. Biophys. Res. Commun.*, 2023, **638**, 134–139.
- 69 A. Singh, A. Torres-Huerta, F. Meyer and H. Valkenier, *Chem. Sci.*, 2024, **15**, 15006–15022.
- 70 S. Benz, M. Macchione, Q. Verolet, J. Mareda, N. Sakai and S. Matile, *J. Am. Chem. Soc.*, 2016, **138**, 9093–9096.
- 71 M. Macchione, M. Tsemperouli, A. Goujon, A. R. Mallia, N. Sakai, K. Sugihara and S. Matile, *Helv. Chim. Acta*, 2018, **101**, e1800014.
- 72 L. Yuan, P. Jiang, J. Hu, H. Zeng, Y. Huo, Z. Li and H. Zeng, *Chin. Chem. Lett.*, 2022, **33**, 2026–2030.
- 73 E. Yashima, N. Ousaka, D. Taura, K. Shimomura, T. Ikai and K. Maeda, *Chem. Rev.*, 2016, **116**, 13752–13990.
- 74 D. Shi, J. Cao, P. Weng, X. Yan, Z. Li and Y. B. Jiang, *Org. Biomol. Chem.*, 2021, **19**, 6397–6401.
- 75 P. Weng, X. Yan, J. Cao, Z. Li and Y. B. Jiang, *Chem. Commun.*, 2022, **58**, 6461–6464.
- 76 M. L. Capobianco, G. Barbarella and A. Manetto, *Molecules*, 2012, **17**, 910–933.
- 77 L. Zhang, N. S. Colella, B. P. Cherniawski, S. C. B. Mannsfeld and A. L. Briseno, *ACS Appl. Mater. Interfaces*, 2014, **6**, 5327–5343.
- 78 S. Kumar, K. Van Hecke and F. Meyer, *Int. J. Mol. Sci.*, 2023, **24**, 11127.
- 79 S. Poplata, A. Tröster, Y. Q. Zou and T. Bach, *Chem. Rev.*, 2016, **116**, 9748–9815.
- 80 G. Berger, L. Fusaro, M. Luhmer, A. Van Der Lee, B. Crousse and F. Meyer, *Tetrahedron Lett.*, 2014, **55**, 6339–6342.
- 81 K. M. Hutchins, J. C. Sumrak and L. R. MacGillivray, *Org. Lett.*, 2014, **16**, 1052–1055.
- 82 W. Yang, D. Zhang, J. Yu and Q. Zhang, *Polym. Chem.*, 2023, **14**, 839–847.
- 83 Q. Wan and B. C. Thompson, *Adv. Sci.*, 2024, **11**, 1–26.
- 84 R. Zhao, T. Zhu, S. Wang, C. Jarrett-Wilkins, A. M. Najjarian, A. J. Lough, S. Hoogland, E. H. Sargent and D. S. Seferos, *Chem. Sci.*, 2022, **13**, 12144–12148.
- 85 A. Facchetti, M.-H. Yoon, C. L. Stern, H. E. Katz and T. J. Marks, *Angew. Chem., Int. Ed.*, 2003, **42**, 3900–3903.
- 86 S. Clément, O. Coulembier, F. Meyer, M. Zeller and C. M. L. Vande Velde, *Acta Crystallogr., Sect. E: Struct. Rep. Online*, 2010, **66**, o896–o897.
- 87 S. Clément, F. Meyer, J. De Winter, O. Coulembier, C. M. L. Vande Velde, M. Zeller, P. Gerbaux, J.-Y. Balandier, S. Sergeev, R. Lazzaroni, Y. Geerts and P. Dubois, *J. Org. Chem.*, 2010, **75**, 1561–1568.
- 88 E. A. Meyer, R. K. Castellano and F. Diederich, *Angew. Chem., Int. Ed.*, 2003, **42**, 1210–1250.
- 89 R. Ferreira De Freitas and M. Schapira, *MedChemComm*, 2017, **8**, 1970–1981.
- 90 J. E. Lee and E. O. Saphire, *Future Virol.*, 2009, **4**, 621–636.
- 91 M. Morales-Tenorio, F. Lasala, A. Garcia-Rubia, E. Aledavood, M. Heung, C. Olal, B. Escudero-Pérez, C. Alonso, A. Martínez, C. Muñoz-Fontela, R. Delgado and C. Gil, *J. Med. Chem.*, 2024, **67**, 16381–16402.
- 92 R. Milani, N. Houbenov, F. Fernandez-Palacio, G. Cavallo, A. Luzio, J. Haataja, G. Giancane, M. Saccone, A. Priimagi, P. Metrangolo and O. Ikkala, *Chem*, 2017, **2**, 417–426.
- 93 F. Meyer, J.-M. Raquez, P. Verge, I. Martínez De Arenaza, B. Coto, P. Van Der Voort, E. Meaurio, B. Dervaux, J.-R. Sarasua, F. Du Prez and P. Dubois, *Biomacromolecules*, 2011, **12**, 4086–4094.
- 94 F. Meyer, J. M. Raquez, O. Coulembier, J. De Winter, P. Gerbaux and P. Dubois, *Chem. Commun.*, 2010, **46**, 5527–5529.
- 95 Y. H. Kwon, J. J. Park, L. M. Housel, K. Minnici, G. Zhang, S. R. Lee, S. W. Lee, Z. Chen, S. Noda, E. S. Takeuchi, K. J. Takeuchi, A. C. Marschilok and E. Reichmanis, *ACS Nano*, 2018, **12**, 3126–3139.
- 96 H. H. AL-Refai, A. A. Ganash and M. A. Hussein, *Mater. Today Commun.*, 2021, **26**, 101935.
- 97 G. Marras, P. Metrangolo, F. Meyer, T. Pilati, G. Resnati and A. Vij, *New J. Chem.*, 2006, **30**, 1397–1402.
- 98 Z. Wang, M. A. Akram, L. Zhao, Z. Liu and Q. J. Niu, *Sep. Purif. Technol.*, 2025, **354**, 129024.
- 99 T. Li, W. Zhu, R. Shen, H. Y. Wang, W. Chen, S. J. Hao, Y. Li, Z. G. Gu and Z. Li, *New J. Chem.*, 2018, **42**, 6247–6255.
- 100 S. Das, P. Heasman, T. Ben and S. Qiu, *Chem. Rev.*, 2017, **117**, 1515–1563.